Raman scattering of $(GaAs)_{n_1}/(AlAs)_{n_2}$ superlattices grown along the [012] direction

Z. V. Popović* and M. Cardona
Max-Planck-Institut für Festkörperforschung, Heisenbergstrasse 1, Postfach 80 06 65, D-7000 Stuttgart 80, Federal Republic of Germany

E. Richter and D. Strauch
Institut für Theoretische Physik, Universität Regensburg, D-8400 Regensburg, Federal Republic of Germany

L. Tapfer and K. Ploog
Max-Planck-Institut für Festkörperforschung, Heisenbergstrasse 1, Postfach 80 06 65, D-7000 Stuttgart 80, Federal Republic of Germany
(Received 2 February 1989)

We report the observation of confined phonon modes in $(GaAs)_{n_1}/(AlAs)_{n_2}$ superlattices grown along the [012] direction. These modes have frequencies which map closely those of the optical phonons of bulk GaAs and AlAs. In near-resonance conditions we observe up to three overtones or combinations of GaAs (AlAs) confined and interface phonons [for a sample with parameters $(n_1,n_2)=(21,25)$ monolayers] or as combinations of only interface modes [for $(n_1,n_2)=(6,42)$ monolayers]. Lattice-dynamical calculations for these superlattices show good agreement with experimentally observed TO and LO confined and interface mode frequencies in the GaAs optical-phonon region.

In recent years theoretical and experimental aspects of semiconductor superlattices have attracted much attention. In these investigations vibrational (mostly Raman) spectroscopy has played a prominent role. The progress in this field has been summarized in several reviews.[1–3] Most studies of GaAs/AlAs superlattices reported so far have been performed on material grown on (001)-oriented GaAs substrates, probably because of the difficulties in preparing high-quality superlattices on other than (001)-oriented substrates. However, recently there has been an increasing interest in the properties of GaAs/AlAs superlattices and quantum wells grown on differently oriented substrates [(110) (Refs. 4 and 5), (111) (Refs. 6 and 7), (310) (Ref. 7), (311) (Ref. 8), and (211) (Ref. 9)]. In this paper we report the observation of confined TO and LO phonons in $(GaAs)_{n_1}/(AlAs)_{n_2}$ superlattices grown along the [012] direction. These phonon modes have frequencies which map closely those of the optical phonons of bulk GaAs and AlAs. We give also a lattice-dynamical calculation for the GaAs/AlAs superlattices used here.

Figure 1 shows a schematic representation of GaAs(AlAs) layers viewed along the [100] direction. The (012) plane, as well as relevant high-symmetry planes, are also indicated.

Superperiodicity in the [012] direction induces a lowering of the crystal symmetry from cubic (T_d) to monoclinic (C_2), the twofold axis (C_2) being parallel to [100], the x axis of GaAs and AlAs layers. In this case the Raman tensor for TO and LO modes, as carried over from those of the bulk crystals, are

$$\begin{bmatrix} 0 & 0 & 0 \\ 0 & 0 & d \\ 0 & d & 0 \end{bmatrix}_{q=0} \quad \text{for the } \mathrm{TO}_x \text{ mode}, \tag{1a}$$

$$\frac{1}{\sqrt{5}} \begin{bmatrix} 0 & d & -2d \\ d & 0 & 0 \\ -2d & 0 & 0 \end{bmatrix}_{q=0} \quad \text{for the } \mathrm{TO}_{\perp x} \text{ mode}, \tag{1b}$$

$$\frac{1}{\sqrt{5}} \begin{bmatrix} 0 & 2d & d \\ 2d & 0 & 0 \\ d & 0 & 0 \end{bmatrix}_{q=0} \quad \text{for the LO mode}. \tag{1c}$$

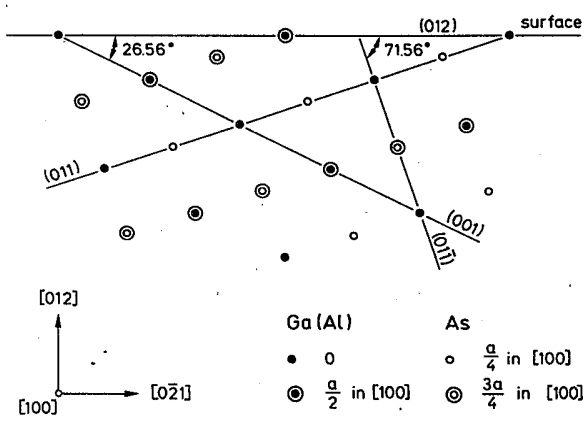

FIG. 1. Schematic representation of the crystal structure of GaAs(AlAs) layers viewed along the [100] direction. The (012) plane as well as other relevant directions are also indicated.

The corresponding Raman polarization rules for the [012] GaAs/AlAs superlattices are given in Table I. Besides the selection rules of the parent material given by Eq. (1), we must consider those arising from the confinement as represented by the corresponding sinusoidal function with wave vector[10–12]

$$q_m=[m/(n_i+1)]\left[\frac{2\pi\sqrt{5}}{a_0}\right]. \tag{2}$$

In the following we distinguish between superlattice wave vector q, bulk wave vector k, and the nominal wave vector q_m of Eq. (2). The $q=0$ modes of the superlattice obtained from Eq. (2) for the m integer have even (A, m even) or odd (B, m odd) symmetry with respect to C_2. For confined modes this symmetry classification remains valid for $q\neq 0$.

The selection rules of Eq. (1) apply for bulk modes of small k along [012]. These modes are mainly longitudinal (LO) or transverse (TO_x or $TO_{\perp x}$) polarized (Fig. 7), and so are the superlattice modes with small q_m. For larger k, bulk modes have mixed transverse-longitudinal character. The eigenvectors of superlattice modes with larger values of q_m have also nonvanishing LO, TO_x, and $TO_{\perp x}$ components. The C_2 symmetry of the superlattice faces the LO, TO_x, and $TO_{\perp x}$ components of a confined optical mode to combine according to the following scheme:

$(\mathrm{LO}, \mathrm{TO}_{\perp x})_m$ for m odd mix, and they also mix with TO_{xm} for m even ; (3a)

$(\mathrm{LO}, \mathrm{TO}_{\perp x})_m$ for m even mix, and they also mix with TO_{xm} for m odd . (3b)

In the following the assignment LO_m, TO_{xm}, or $\mathrm{TO}_{\perp xm}$ to a superlattice mode is to be understood as relating to the main polarization and Fourier component of the calculated eigenvectors. Hence an exact correspondence of the observed frequencies with those obtained from the bulk dispersion relation using Eq. (2), as found for [001] superlattices, is not expected. We note that, in addition to Eq. (1), we must also include the Raman tensor resulting from the "dipole-forbidden" Fröhlich interaction of LO phonons of even m (A symmetry). It should also contribute to scattering by TO phonons of large q because of the mixing discussed above. These components appear automatically as allowed contributions to the Raman tensors for the general C_2 symmetry of the superlattice.

The samples studied here are four GaAs/AlAs superlattices grown on [012]-oriented undoped semi-insulating GaAs substrates by molecular-beam epitaxy. Details of the growth procedure and x-ray characterization of the samples studied here are given in our earlier paper.[13] Briefly, the growth temperature was $T_s\sim 550\,^\circ\mathrm{C}$ and the growth rate as low as one monolayer per sec. The samples consist of 100–150 periods of alternating GaAs and AlAs layers. The constituent layer thicknesses are represented by the number of GaAs (n_1) and AlAs (n_2) monolayers, each monolayer being 1.263 Å thick. The actual superlattice period of the samples was measured with a computer-controlled high-resolution double crystal x-ray diffractometer.

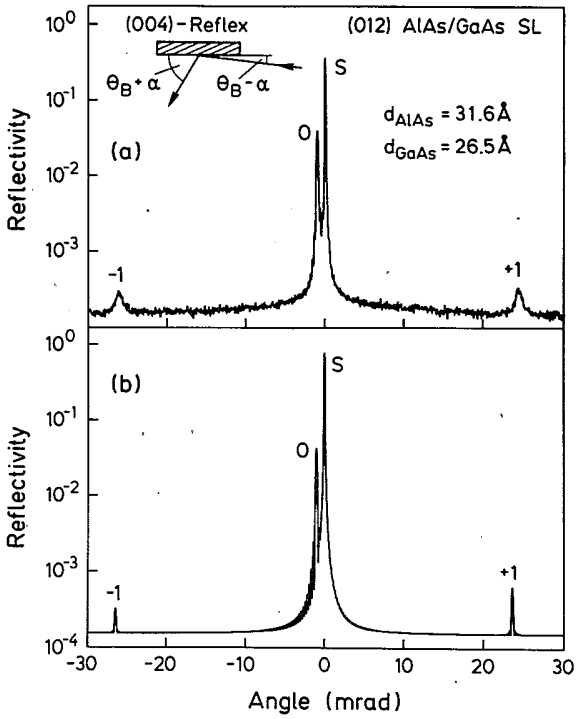

FIG. 2. X-ray diffraction pattern in the vicinity of the (004) Cu $K\alpha_1$ reflection of the (012) $(GaAs)_{21}/(AlAs)_{25}$ superlattice. (a) Experimental and (b) calculated diffraction curve.

Figure 2(a) shows the (004)-diffraction pattern for a (012) $(GaAs)_{21}/(AlAs)_{25}$ superlattice with $\gamma_0<\gamma_h$,[14] where $\gamma_0=\cos[\pi/2-(\Theta_B-\alpha)]$ and $\gamma_h=\cos[\pi/2-(\Theta_B+\alpha)]$ are the direction cosines of the diffracted beam, Θ_B is the kinematical (004) Bragg angle, and α is the angle between the (001) and (012) planes. The spectrum exhibits the main superlattice peak (0) close to the substrate peak S, and both are well resolved. Their separation re-

TABLE I. Raman polarization selection rules in backscattering geometry for GaAs/AlAs superlattices grown along the [012] direction as carried over from those for the bulk crystal; a represents intraband Fröhlich and d deformation potential terms. The mixing indicated in Eq. (3) will modify these selection rules for large values of q_m [Eq. (2)].

Configuration	Incident polarization	Scattering polarization	Raman cross section A	Raman cross section B
$\bar{z}(xx)z$	[100]	[100]	a^2	0
$\bar{z}(y'x)z$	[0$\bar{2}$1]	[100]	0	$\frac{9}{25}d^2(\mathrm{LO})+\frac{16}{25}d^2(\mathrm{TO}_{\perp x})$
$\bar{z}(y'y')z$	[0$\bar{2}$1]	[0$\bar{2}$1]	$a^2+\frac{16}{25}d^2(\mathrm{TO}_x)$	0

veals pseudomorphic growth without strain release at the GaAs/AlAs interfaces. The first two satellite peaks are also clearly seen. Figure 2(b) shows, for comparison, the calculated diffraction pattern of this superlattice assuming pseudomorphic growth. The appearance of distinct satellite peaks and the very good agreement between the experimental and calculated data demonstrates the high structural quality of the specimen. The slight broadening of the observed satellite peaks indicates a small interface roughness (1–2 monolayers) at the GaAs/AlAs and AlAs/GaAs transition region.[14] X-ray diffraction on the other samples yielded the parameters $(n_1,n_2)=(14,16)$, (6,42), and (23,8).

The Raman spectra were measured in backscattering geometry using a Spex Industries double monochromator with a conventional photon-counting detection system. The excitation sources were the 5145-Å line of an Ar^+-ion laser and 6471- and 6764-Å lines of a Kr^+-ion laser. Measurements were made both at room and at liquid-nitrogen temperatures.

Figure 3(a) shows Raman spectra for the $(GaAs)_{21}/(AlAs)_{25}$ superlattice in the spectral region corresponding

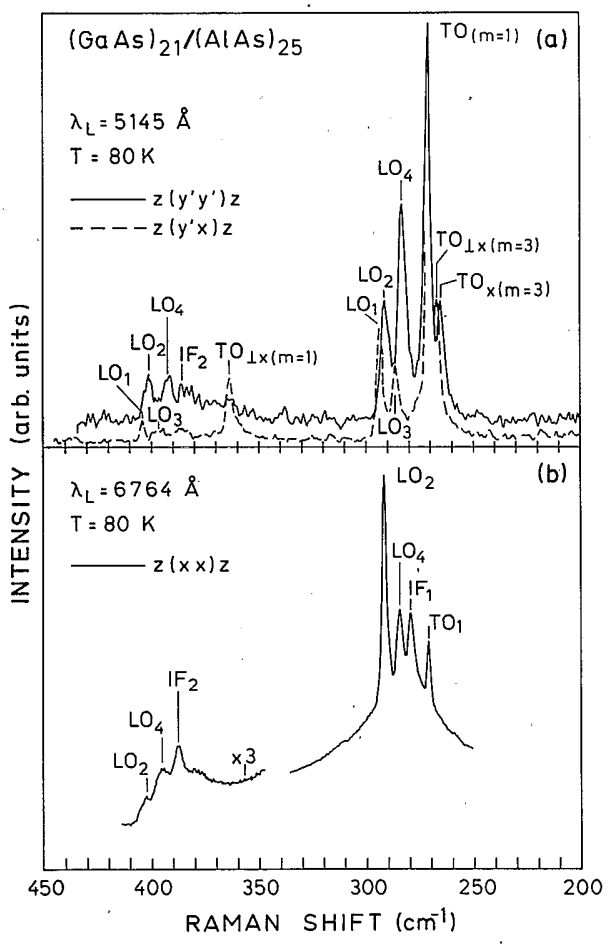

FIG. 3. Raman spectra of a $(GaAs)_{21}/(AlAs)_{25}$ superlattice at 80 K in backscattering configuration ($x=[100]$, $y'=[0\bar{2}1]$, $z=[012]$). (a) Exciting laser line $\lambda_L=5145$ Å away from all resonances; (b) exciting laser line $\lambda_L=6764$ Å near resonance condition. In this case the Raman spectra are the same for polarized and depolarized configurations.

to the optical phonons of GaAs and AlAs, obtained at 80 K with the laser line $\lambda_L=5145$ Å away from all resonances. Figure 3(b) includes the same spectral region for near-resonance conditions with the first electron–heavy-hole exciton of the GaAs layers. The off-resonance spectra are different for the polarized $\bar{z}(y'y')z$ and depolarized $\bar{z}(y'x)z$ configurations, as expected from selection rules given in Table I [note that the mixing of Eq. (3) is neglected in Table I]. The depolarized spectra should correspond mainly to B and the polarized ones mainly to A modes. The peaks labeled LO_m correspond to the confined longitudinal optical modes localized in the GaAs and AlAs slabs. Besides LO_m confined phonons, TO_m confined modes are also shown in Fig. 3(a). For $m=1$, we cannot resolve the GaAs TO_{xm} and $TO_{\perp xm}$ modes, while, for $m=3$, these modes differ by about 2 cm^{-1}. The difference between TO_{xm} and $TO_{\perp xm}$ modes in the AlAs side is also difficult to resolve because the TO_{xm} modes are weak. It is, however, possible to conclude that the $TO_{\perp x1}$ mode has a higher frequency than TO_{x1}, in agreement with phonon-dispersion curves for these modes [see Fig. 7(c), below].

Near resonance the A modes become dominant for all polarizations.[15,16] The two additional lines in Fig. 3(b), located at 278 and 385 cm^{-1}, and labeled IF_1 and IF_2, are attributed to interface modes.[17]

A Raman spectrum of the same sample obtained at 80 K with the 6471-Å line in the spectral range from 200–1000 cm^{-1} is displayed in Fig. 4. This laser line is again very close to resonance, and we observe up to three-phonon overtones in the regions of GaAs and AlAs zone-center phonons. An interesting feature is that all GaAs higher-order peaks can be explained only as a combination of A modes (m even), and almost all higher-order peaks are a combination of GaAs (AlAs) confined modes with the LO_2 GaAs (AlAs) mode. Due to the absence of B modes in the first-order spectrum and of combinations of B modes with A modes in higher-order spectra, we conclude that modes observed in resonance are determined by the Fröhlich electron-phonon interaction.[16]

Figure 5 shows Raman spectra of the $(GaAs)_{14}/(AlAs)_{16}$ superlattice at 300 K for $(y'y')$ and $(y'x)$ polarization. The LO_1 and LO_2 modes of the GaAs side can be readily identified. The LO_3 and LO_4 modes cannot be resolved because of the overlap with a TO mode. In the AlAs spectral region, besides LO_1 and LO_2 confined phonons, we observed TO_x and $TO_{\perp x}$ ($m=1$) modes at 362 and 363 cm^{-1}, and a weak mode at about 385 cm^{-1} in both polarizations. We assign it to an interface mode (IF_2).

Raman spectra of the $(GaAs)_6/(AlAs)_{42}$ superlattice are given in Fig. 6. Figure 6(a) shows first- and higher-order Raman spectra for $(y'y')$ polarization obtained at 80 K using the 5145-Å line. Higher-order spectra are the same for all polarizations, while one-phonon spectra are different for $(y'y')$ and $(y'x)$ polarization as shown in Fig. 6(b). In the GaAs optical phonon region we observe four modes at 282, 278, 270, and 268 cm^{-1}. We believe that the modes at 282 and 268 cm^{-1} for the depolarized

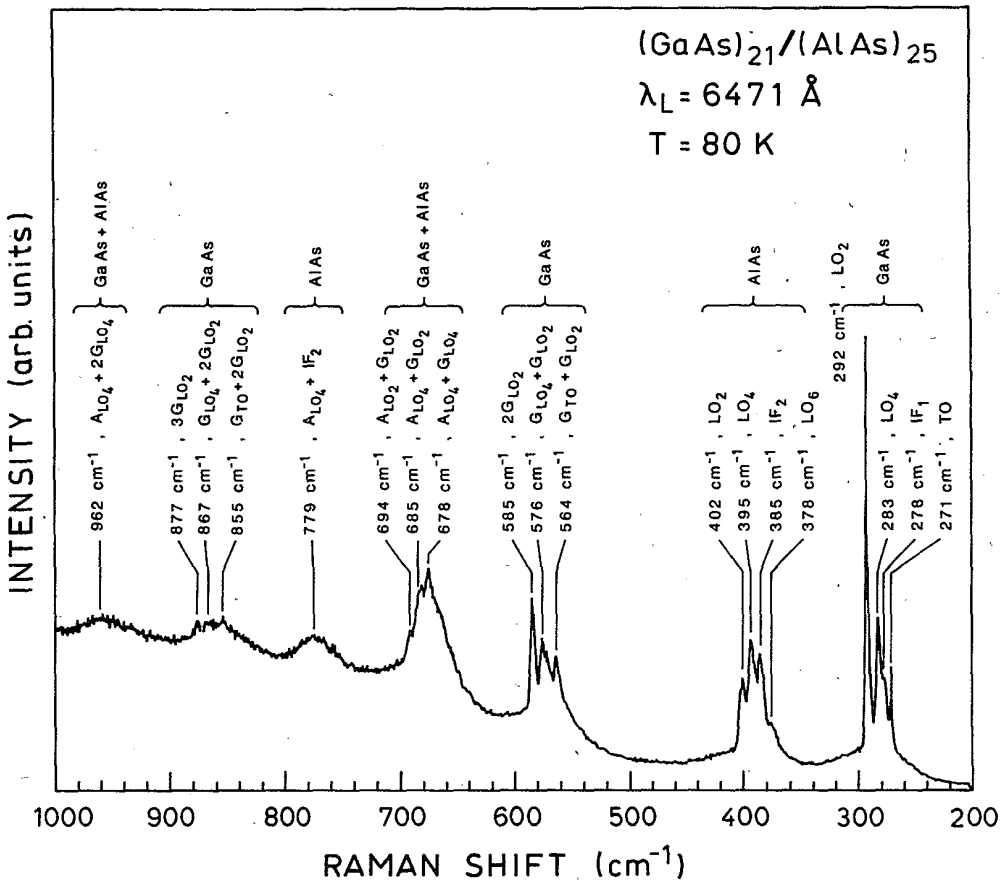

FIG. 4. Raman spectra of a $(GaAs)_{21}/(AlAs)_{25}$ superlattice at 80 K in the $z(xx)z$ configuration. Exciting laser line $\lambda_L = 6471$ Å very close to resonance conditions. The rise at higher energy is due to photoluminescence.

configuration are LO_1 and $TO_{\perp x1}$ confined modes. The strongest mode for the polarized configuration is at 278 cm^{-1}. This mode is also present for the $(y'x)$ polarization. It cannot be a confined mode since its frequency falls well above that of the LO_2 confined mode [Fig. 7(b)];

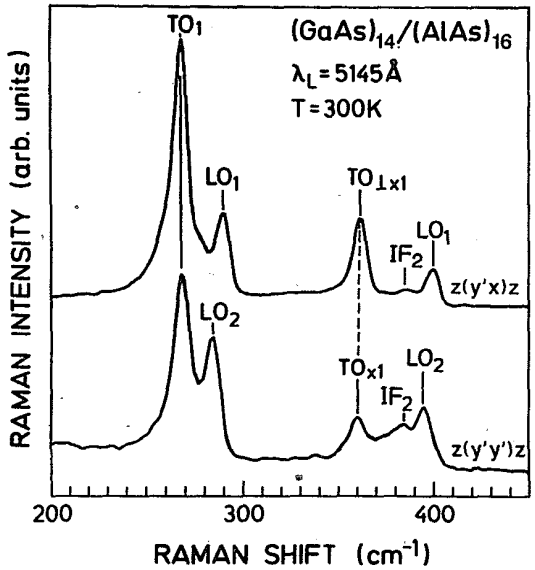

FIG. 5. Raman spectra of a $(GaAs)_{14}/(AlAs)_{16}$ superlattice at 300 K in the $z(y'y')z$ and $z(y'x)z$ configuration using the 5145-Å line of an Ar^+ laser.

we conclude that it is an interface mode. The next mode for $(y'y')$ polarization, at 270 cm^{-1}, could be the LO_2 confined mode. For $(y'y')$ polarization, we also expect to see the TO_{x1} mode (at frequencies lower than $TO_{\perp x1}$), but it cannot be clearly resolved, probably because it overlaps with the stronger LO_2 mode. Detailed assignment of these LO and interface modes as well as other modes of the $(GaAs)_6/(AlAs)_{42}$ sample will be given after discussion of the calculated phonon-dispersion curves of GaAs and AlAs in the [012] direction and the lattice dynamics of this superlattice.

The strongest line in the AlAs optical-phonon region appears for both polarizations at 394 cm^{-1}. Following the interpretation of Sood *et al.*,[17] we assign it also to an interface mode. The other feature in this spectral region, at about 402 cm^{-1}, is an LO_2 confined mode. The frequency difference between LO_1 [for $(y'x)$ polarization] and LO_2 [for $(y'y')$ polarization] confined phonons is not detected because the LO branch of AlAs is practically flat between q_1 (=0.023) and q_2 (=0.046) [in units of $(2\pi\sqrt{5}/a_0)$].

The higher-order spectra shown in Fig. 6(a) can be explained as combinations, not from different phonon branches, as in Fig. 4 for $(GaAs)_{21}/(AlAs)_{25}$ samples, but from phonons of different materials. In particular, only combinations of interface modes are observed. Similar results were recently reported[18] for GaAs/AlAs superlattices grown along the [001] direction.

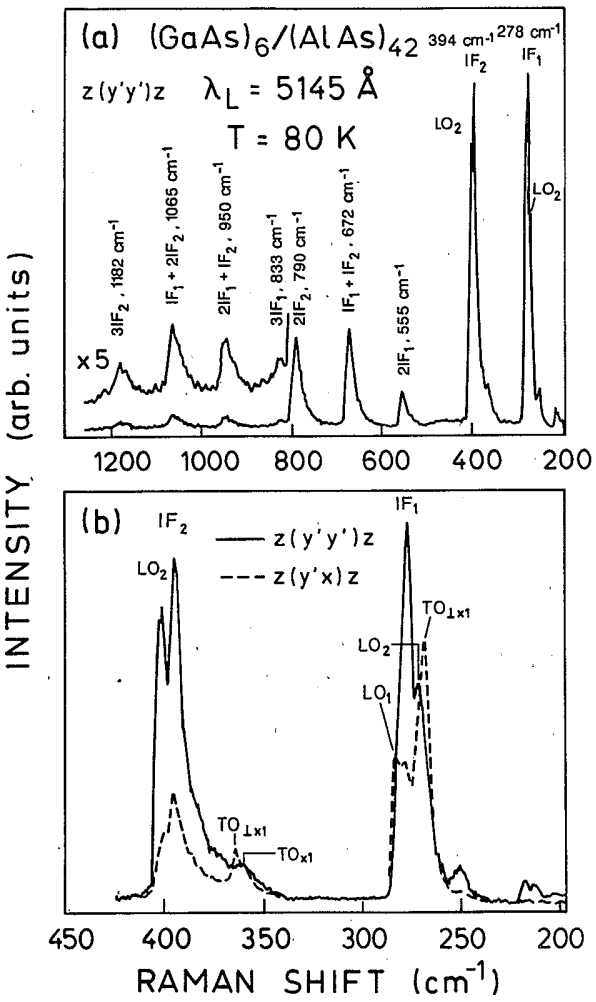

FIG. 6. Raman spectra of a $(GaAs)_6/(AlAs)_{42}$ superlattice at 80 K using the 5145-Å line at an Ar^+ laser near resonance condition. (a) First- and higher-order spectra in the $\bar{z}(y'y')z$ configuration; (b) first-order spectra in the $\bar{z}(y'y')z$ and $\bar{z}(y'x)z$ configuration.

Figure 7(a) shows the phonon-dispersion curves in GaAs and AlAs for wave vectors along the $\Gamma-W-X$ direction calculated using the valence overlap shell model (VOSM).[19] For GaAs we selected parameters of VOSM that gave the best fit to recent low-temperature high-precision neutron data.[19] The phonon-dispersion curves of AlAs were described by the same model with only the mass of the cation being changed.

Using the assignment of the observed Raman peaks to confined LO and TO phonon modes, as discussed above, we compare the corresponding frequencies with the dispersion relations of bulk GaAs and AlAs. Figures 7(b) and 7(c) show the measured frequencies of LO_m, $TO_{\perp xm}$, and TO_m phonons versus $q_m=[m/(n_i+1)](2\pi\sqrt{5}/a_0)$, together with the optical-phonon-dispersion curves of bulk GaAs and AlAs. In the same figures are plotted the projections of the phonon eigenvectors along the three directions ([012], [0$\bar{2}$1], [100]) at several phonon frequencies for all optical branches. The projections plotted are the corresponding components of

$$\mathbf{e}_{j_a}(q)/\sqrt{m_a}-\mathbf{e}_{j_c}(q)/\sqrt{m_c}\ , \qquad (4)$$

where $\mathbf{e}_{j_{a,c}}(q)$ and $m_{a,c}$ are eigenvectors components and masses of anion and cation. This representation aids the identification of the dominant character of the vibrations and clearly exemplifies the low symmetry of the system: for $k\neq 0$ all modes are of mixed (LO,TO) character, since the group of the **k** vector contains only the identity. In order to relate a nominal wave vector q_m to a bulk **k** vector, we neglect the fact that, because of the odd-even combination of Eq. (3), the layer modes (standing waves) cannot correspond exactly to bulk running waves. The mixing of the superlattice modes will be considered in detail below.

For GaAs optical phonons, as seen from Fig. 7(b), the agreement between our experimental data and the theoretical predictions is excellent. The largest difference (4 cm^{-1}) between phonon-dispersion curves and experimental data in the GaAs optical phonon region is for the LO_1 mode of the $(GaAs)_6/(AlAs)_{42}$ sample at about 282 cm^{-1}. This difference may be due to mixture of this mode with TO modes. In Fig. 6(b) there is an unidentified peak at about 250 cm^{-1} for $(y'y')$ polarization. This mode may be a confined mode from the lower phonon branch for $q_{m=2}$ [this mode, as indicated in Fig. 7(b), has predominantly LO character]. For the optical phonons of AlAs we have the same type of dependence of confined mode frequencies versus q and of theoretical phonon-dispersion curves. The largest difference between experimental and theoretical data is about 6 cm^{-1} in the AlAs region. For bulk AlAs there are no neutron scattering data available; hence this difference may originate from insufficient accuracy of the calculated dispersion curves of bulk AlAs. Our value of 404 cm^{-1} for $LO(\sim\Gamma)$ is in very good agreement with the value of $LO(\Gamma)$ from recently published Raman scattering data[20] for a (001) GaAs/AlAs superlattice.

Finally, in Fig. 8 we compare our Raman spectra in the GaAs optical-phonon region of the samples with (n_1,n_2) equal (21,25) and (6,42) with a theoretical calculation for these superlattices. Realistic phonon properties of these superlattices are determined by using three-dimensional shell-model calculations previously described in Ref. 21. We have calculated eigenfrequencies and eigenvectors of the modes with $q_\perp=0$ (solid lines in Fig. 8) and also the interface modes of these structures: their frequencies are denoted by dashed and chain-dotted lines for interface mode propagating in [100] and [0$\bar{2}$1] directions. For the AlAs interface mode we obtained the values of 385 and 392 cm^{-1} for (21,25) and (6,42), in good agreement with our experimental finding.

As can be seen from Fig. 8(a), the agreement between experimental data and theoretical calculations for GaAs-like confined optical phonons of the $(GaAs)_{21}/(AlAs)_{25}$ superlattice is rather good. Through this comparison it is also possible to explain the large intensity of the LO_4 mode as a superposition with interface modes at about 282.5 cm^{-1} propagating in both the [100] and [0$\bar{2}$1] directions. Also, the shoulders in the Raman spectra for the $(y'y')$ polarization at 289, 279, and 276 cm^{-1} can originate from interface modes in both or one of the [100] and [0$\bar{2}$1] directions, as indicated in Fig. 8(a). The dom-

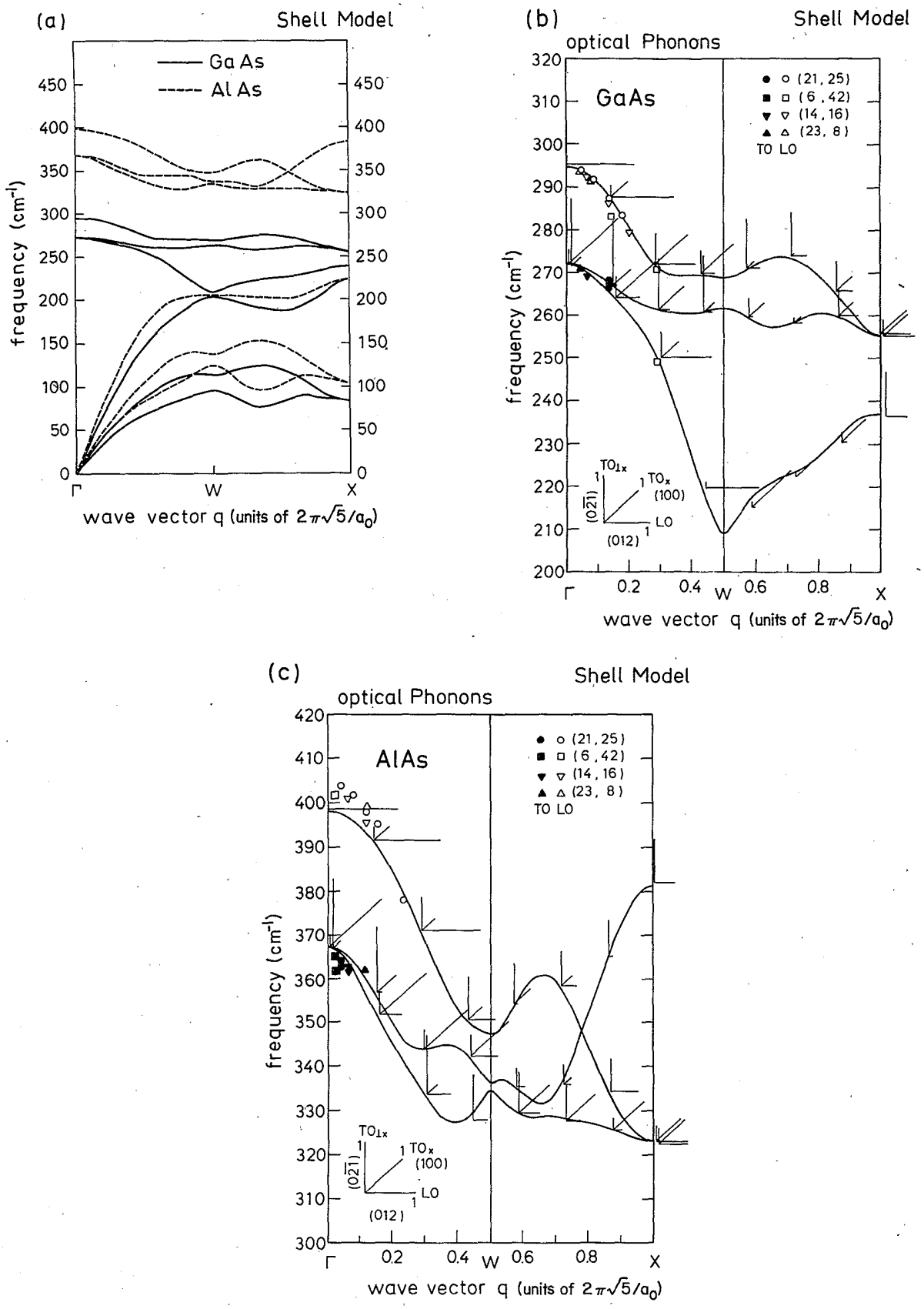

FIG. 7. (a) Phonon-dispersion curves of GaAs and AlAs in the $\Gamma-W-X$ direction. (b),(c) Experimental confined mode frequencies as a function of confinement wave vector $q_m=[m/(n_i+1)](2\pi\sqrt{5}/a_0)$ together with theoretical optical-phonon-dispersion curves of bulk GaAs and AlAs, and the projections of the corresponding phonon displacements of the cation relative to the nearest anion [Eq. (4)] along the [012], [0$\bar{2}$1], and [100] directions.

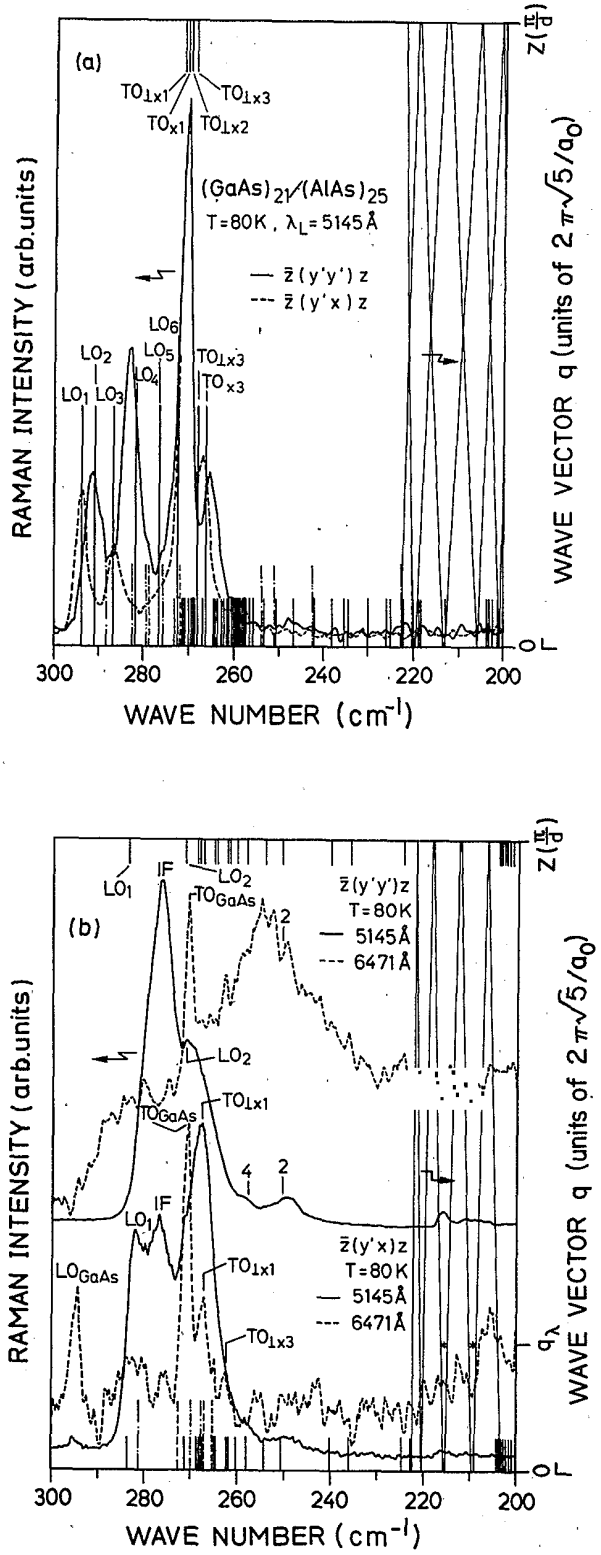

FIG. 8. Comparison of Raman spectra in the GaAs optical-phonon region with lattice-dynamical calculation for (a) $(GaAs)_{21}/(AlAs)_{25}$ and (b) $(GaAs)_6/(AlAs)_{42}$ superlattices. The positions of calculated confined phonons are represented by vertical solid lines. Interference modes are represented with chain dotted and dashed lines: $-\cdot\cdot-$ *IF* mode in $[0\bar{2}1]$ direction; $- - -$ *IF* mode propagating in [100] direction; $-\cdot-\cdot-$ *IF* modes in both the $[0\bar{2}1]$ and [100] directions.

inant features in the Raman spectra on Fig. 8(a) are $TO_{x(m=1)}$ and $TO_{\perp x(m=1)}$ modes at about 271 cm^{-1}. The calculations give frequencies of 271.6 cm^{-1} for $m=1$, and 270 cm^{-1} for $m=2$ for the $TO_{\perp x}$, and 270.91 cm^{-1} ($m=1$) for the TO_x mode. Because the frequency of the $m=2$ TO confined modes is very close to that of the $m=1$ TO, they cannot be resolved. Therefore, we assign the resolved peaks at 267 and 265 cm^{-1} to $TO_{\perp x}$ and TO_x confined modes for $m=3$. This assignment is in good agreement with our calculated frequencies: 268.2 cm^{-1} ($TO_{\perp x3}$ mixed with LO_3+TO_{x4}) and 266.3 cm^{-1} (TO_{x3} mixed with $TO_{\perp x4}+LO_4$) as indicated in Fig. 8(a). The other calculated superlattice modes shown in Fig. 8(a) cannot be resolved due to their weak intensity.

A comparison of the calculated superlattice optical modes with the Raman spectra of the $(GaAs)_6/(AlAs)_{42}$ superlattice is given in Fig. 8(b). The solid lines represent Raman spectra measured with the 5145-Å line of an Ar^+-ion laser (as in Fig. 6) and the dashed lines are the same spectra obtained by using the 6471-Å line of a Kr^+-ion laser. There is a large difference between these spectra. Raman spectra measured with the 5145-Å line have strong intensities and display many overtones because they are in resonance, and Raman spectra obtained with the 6471-Å line have weak intensity and considerable noise. According to our preliminary photoluminescence (PL) spectra measured at 80 K, this sample has a weak luminescence peak at about 2.32 eV and a 60 times stronger one at about 1.9 eV. These peaks originate from direct and indirect gaps (transition to hole states at the Brillouin-zone center in GaAs from the electron state at Γ and X maxima in AlAs). Their energies are in agreement with the values of corresponding energies of [001] GaAs/AlAs superlattices with nearly the same GaAs (AlAs) -layer thicknesses.[22] Enhancement of the Raman spectra was found only at the energy of about 2.41 eV (near the first electron–heavy-hole exciton of the GaAs layer). As mentioned above, no enhancement of Raman spectra was found with the laser line (6471 Å) near the energy of the indirect transition. The largest different between the spectra given in Fig. 8(b) is in the interface mode at about 278 cm^{-1}, which is present only in resonance. As can be seen from Fig. 8(b), the frequency of this mode falls between the LO_1 and LO_2 confined modes. The next mode for $(y'y')$ polarization is at 270 cm^{-1}. We have assigned it to the LO_2 confined mode. In fact, this mode is mixed with the TO_x and $TO_{\perp x}$ modes according to the scheme mentioned above ($LO_2+TO_{\perp x2}+TO_{x1}$), and has predominantly LO character. Two other shoulders at about 260 and 250 cm^{-1} (denoted in Fig. 8(b) by 4 and 2) are also mixed modes with predominantly $TO_{\perp x}$ and LO character. The interface mode is missing in the out of resonance Raman spectra: the dominant feature is the sharp GaAs TO mode arising from the substrate. There are some very weak confined modes in the spectral range between 265 and 250 cm^{-1}, whose existence is also predicted by the calculations. The last two shoulders for the $(y'y')$ polarization probably come from the longitudinal acoustic phonon branch; the calculations predict the existence of folded phonons at 216 and 210

cm^{-1}, as indicated by the asterisks in Fig. 8(b).

For the $(y'x)$ polarization, LO_1 and $TO_{\perp x1}$ confined phonon modes are clearly observed at 282 and 268 cm^{-1}; our calculations for these modes give the frequencies of 283.8 and 267.7 cm^{-1}. Out of resonance for this polarization, besides bulk TO and LO GaAs modes, the modes with predominantly $TO_{\perp x1}$ and $TO_{\perp x3}$ character are also observed, at frequencies in good agreement with the theoretical prediction.

According to our x-ray and photoluminescence measurements, the (6,42) superlattice has more disorder than the (21,25) superlattice; namely, the interface roughness for the (6,42) sample was found to be about two monolayers, which is twice that for the other superlattices studied here. We believe that this may be responsible for the strong, and otherwise forbidden, coupling to modes propagating along the interfaces.

We consider now the effect of mixing on the frequency shift of the (012) GaAs/AlAs superlattice modes. Figure 9 shows the calculated frequencies of GaAs confined modes versus $q_m=[m/(n_i+1)](2\pi\sqrt{5}/a_0)$ for all samples studied here, together with phonon-dispersion curves of bulk GaAs in the [012] direction. We note that because of the m =odd-even mixing [Eq. (3)], the frequencies of the superlattice modes should not fall exactly on the dispersion curves of bulk GaAs, in contrast to the case of (001) (Ref. 21) and (110) (Ref. 4) GaAs/AlAs superlattices. Note that for a (110)-oriented superlattice, only the $TO_{\perp z}$ phonon branch is pure and the other two (LO and TO_z branches) are also mixed. The effect of mixing is thus different for different optical phonon branches $\omega_j(q)$ $(j=1,2,3)$ and different thicknesses (number of monolayers n_i) of the superlattices. We present in Fig. 9 a calculation of the effect of mixing on the mapping of superlattice modes on bulk modes.

The superlattice modes which correspond to the highest $[\omega_1(q)]$ phonon branch in Fig. 9 [with predominantly LO character for $q<0.25$ in units of $(2\pi\sqrt{5}/a_0)$] have lower frequencies than the bulk modes, possibly because of mixing with the other two branches. This difference is largest for the shortest period superlattices sample $(n_i=6)$ [in addition, the assignment of an effective wave vector q_m, as in Eq. (2), to the confined modes of such a small period layer may not be completely justified]. The strongest mixing should take place in the region between 260 and 272 cm^{-1}, where there are modes in all three dispersion branches. Because of this strong mixing, it was not always possible to assign the corresponding confined wave vector to a given m and to identify the predominant character of these modes; in particular, for the $\omega_2(q)$ phonon branch for $q>0.5$. The highest-frequency difference between the superlattice modes and the bulk dispersion curves exists also for the $\omega_3(q)$ phonon branch for $q>0.5$, as a consequence of mixing with higher-energy bands of different m. The differences are small, however, in spite of the m odd-even mixing. In the long-period $(n\geq 14$ monolayer) (012) superlattices, the mode mixing plays a relatively minor role.

In summary, we have investigated the Raman spectra of GaAs/AlAs superlattices grown along the [012] direction, and observed confined TO and LO phonon modes with frequencies close to those predicted from the phonon dispersion of bulk GaAs and AlAs in the $\Gamma-W-X$ direction. In near-resonance conditions we observe higher-order spectra as combinations of confined phonons of type A for a (21,25) superlattice and combination of interface phonons for a (6,42) superlattice. Calculations of the lattice dynamics of the superlattices studied show good agreement with the experimental data for TO and LO confined and interface modes in the GaAs optical phonon region.

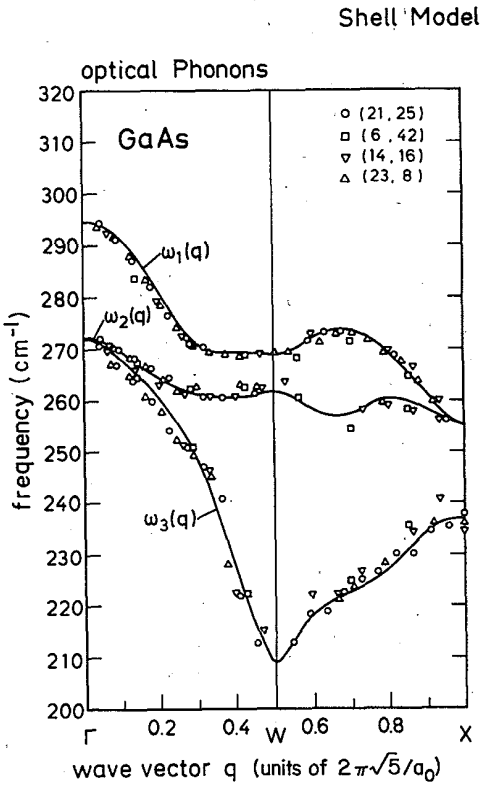

FIG. 9. Optical phonon-dispersion curves of bulk GaAs in the [012] direction of k space, together with calculated frequencies of superlattice confined modes vs $q_m=[m/(n_i+1)](2\pi\sqrt{5}/a_0)$ for all samples studied here.

We would like to thank A. Alexandrou and W. Stolz for some of the photoluminescence measurements. The technical assistance of A. Fisher with molecular-beam-epitaxy growth, and of H. Hirt, M. Siemers, and P. Wurster with Raman measurements is gratefully acknowledged. Part of this work was sponsored by the Bundesministerium für Forschung und Technologie of the Federal Republic of Germany. One of us (Z.V.P.) was supported by the Alexander von Humboldt Foundation (Bonn, Federal Republic of Germany).

*Permanent address: Institute of Physics, P.O. Box 57, YU-11000 Belgrade, Yugoslavia.

[1]M. V. Klein, IEEE J. Quantum Electron. **QE-22**, 1760 (1986).

[2]M. Cardona, in *Lectures on Surface Science, Proceedings of the Fourth Latin-American Symposium,* edited by G. R. Castro and M. Cardona (Springer-Verlag, Berlin, 1987), p. 2.

[3]B. Jusserand and M. Cardona in *Light Scattering in Solids V,* edited by M. Cardona and G. Güntherodt (Springer-Verlag, Heidelberg, 1989), p. 49.

[4]Z. V. Popović, M. Cardona, E. Richter, D. Strauch, L. Tapfer and K. Ploog, Phys. Rev. B (to be published).

[5]D. Kirillov and Y. C. Pao, in *Materials Research Society Symposium Proceedings* (MRS, Pittsburgh, 1988), Vol. 102, p. 169.

[6]T. Hayakawa, K. Takahashi, M. Kondo, T. Suyama, S. Yamamoto, and T. Hijikata, Phys. Rev. Lett. **60**, 349 (1988).

[7]L. W. Molenkamp, G. E. W. Bauer, R. Eppenga, and C. T. Foxon, Phys. Rev. B **38**, 6147 (1988).

[8]T. Fukunaga, T. Takamori, and H. Nakashima, J. Cryst. Growth **81**, 85 (1987).

[9]S. Subbanna, H. Kroemer, and J. L. Merz, J. Appl. Phys. **59**, 488 (1986).

[10]E. Molinari, A. Fasolino, and K. Kunc, Phys. Rev. Lett. **56**, 1751 (1986).

[11]B. Jusserand and D. Paquet, Phys. Rev. Lett. **56**, 1752 (1986).

[12]A. K. Sood, J. Menéndez, M. Cardona, and K. Ploog, Phys. Rev. Lett. **56**, 1753 (1986).

[13]Z. V. Popović, M. Cardona, L. Tapfer, K. Ploog, E. Richter, and D. Strauch, Appl. Phys. Lett. **54**, 846 (1989).

[14]L. Tapfer and K. Ploog, Phys. Rev. B **33**, 5565 (1986).

[15]A. K. Sood, J. Menéndez, M. Cardona, and K. Ploog, Phys. Rev. Lett. **54**, 2111 (1985).

[16]A. Alexandrou, M. Cardona, and K. Ploog, Phys. Rev. B **38**, 2198 (1988).

[17]A. K. Sood, J. Menéndez, M. Cardona, and K. Ploog, Phys. Rev. Lett. **54**, 2115 (1985).

[18]M. H. Meynadir, E. Finkman, M. D. Sturge, J. M. Worlock, and M. C. Tamargo, Phys. Rev. B **35**, 2517 (1987).

[19]D. Strauch and B. Dorner (unpublished). The lattice-dynamical model is that of G. Dolling and J. L. T. Waugh, in *Lattice Dynamics,* edited by R. F. Wallis (Pergamon, Oxford, 1965), p. 19.

[20]Z. P. Wang, D. S. Jiang, and K. Ploog, Solid State Commun. **65**, 661 (1988).

[21]E. Richter and D. Strauch, Solid State Commun. **64**, 867 (1987).

[22]G. Danan, B. Etienne, F. Mollot, R. Planel, A. M. Jean-Louis, F. Alexandre, B. Jusserand, G. Le Roux, J. Y. Marzin, H. Savary, and B. Sermage, Phys. Rev. B **35**, 6207 (1987).